

Evaluation of Series Resistance Losses in Screen-Printed Solar Cells With Local Rear Contacts

Sebastian Gatz, Thorsten Dullweber, and Rolf Brendel

Abstract—We demonstrate industrially feasible large-area solar cells with passivated homogenous emitter and rear achieving energy conversion efficiencies of up to 19.4% on 125 mm × 125 mm p-type 2–3-Ω·cm boron-doped Czochralski silicon wafers. Front and rear metal contacts are fabricated by screen printing of silver and aluminum paste and firing in a conventional belt furnace. However, these cells suffer from moderate fill factors below 76% due to an increased series resistance. In this paper, we analyze the main cause of this increase. We vary the rear contact geometry over a wide range. By subtracting the respective contribution of the base from the measured series resistance, we extract a value of $(55 \pm 10) \text{ m}\Omega\cdot\text{cm}^2$ for the effective specific contact resistivity of our screen-printed local aluminum rear contacts. We verify this value by local series resistance mappings from photoluminescence measurements resulting in a contact resistivity of $(40 \pm 10) \text{ m}\Omega\cdot\text{cm}^2$. Our analysis reveals that the highest potential for a further energy conversion efficiency improvement is to decrease the rear contact resistivity.

Index Terms—Photovoltaics, resistance, silicon, solar cells.

I. INTRODUCTION

THE TREND in the industrial silicon (Si) solar cell production toward thinner wafers in combination with the aim of higher energy conversion efficiencies demands an improved rear surface passivation. A conventional screen-printed aluminum (Al) back-surface field (BSF) shows a moderate passivation quality with typical rear surface recombination velocities S_{rear} ranging from 200 to 600 cm/s on 1–3-Ω·cm p-type silicon [1], [2]. The passivated emitter and rear solar cell (PERC) applies dielectric passivation layers to the front and rear [3]. At the cell rear, a significantly better passivation performance is achieved by dielectric layers compared with the full-area Al-BSF. The additional dielectric layer also improves the internal rear reflectance that reduces absorption losses in the Al back contact. At the Institute for Solar Energy Research Hamelin (ISFH), Emmerthal, Germany, we recently demonstrated a 19.4% efficient screen-printed PERC solar cell [4].

Manuscript received July 5, 2011; revised July 28, 2011; accepted July 29, 2011. Date of publication August 30, 2011; date of current version October 27, 2011.

S. Gatz and T. Dullweber are with the Institute for Solar Energy Research Hamelin, D-31860 Emmerthal, Germany (e-mail: s.gatz@isfh.de; t.dullweber@isfh.de).

R. Brendel is with the Institute for Solar Energy Research Hamelin, D-31860 Emmerthal, Germany, and also with the Department of Solar Energy, Institute of Solid-State Physics, Leibniz University of Hanover, D-30167 Hannover, Germany (e-mail: r.brendel@isfh.de).

Color versions of one or more of the figures in this paper are available online at <http://ieeexplore.ieee.org>.

Digital Object Identifier 10.1109/JPHOTOV.2011.2163925

However, our record PERC cells suffer from moderate fill factors below 76% due to an increased series resistance.

Generally, the contribution to the series resistance associated with the contact resistance is given by

$$R_{c,\text{rear}} = \frac{\rho_c}{f_{\text{rear}}} \quad (1)$$

with the metallization fraction f_{rear} , where the effective specific contact resistivity ρ_c is independent of the contact size.

Melczarsky *et al.* [5] investigated contact resistance samples where the Al paste is printed directly on the Si surface. They showed that the contact resistance associated with the screen-printed aluminum/silicon interface is inversely proportional to the contact area A_{cont} . Rohatgi *et al.* [6] showed that applying an Al paste fired on bare Si provides a specific contact resistivity $\rho_c = 10 \text{ m}\Omega\cdot\text{cm}^2$ on 2.3-Ω·cm wafers. However, Urrejola *et al.* [7] reported about a different behavior in contact measurements with a PERC structure. Screen-printed aluminum fingers were deposited on top of locally opened dielectric layers. Investigations applying the transmission line model reveal that the specific contact resistivity depends on the contact area, where the Al–Si alloy is formed.

In this paper, we determine the effective specific contact resistivity at the rear $\rho_{c,\text{rear}}$ of screen-printed PERC solar cells deduced from two different series resistance measurement approaches. The first is based on current–voltage investigations; the second is based on photoluminescence (PL) measurements.

II. SOLAR CELL PROCESS

We process the solar cells based on the process flow presented in [4]. However, during several cell runs, we modify various process parameters over a wide range. The 125 mm × 125 mm solar cells are fabricated on 200-μm-thick 2–3-Ω·cm p-type boron-doped Czochralski (Cz)-silicon wafers. Fig. 1 shows the process flow; Fig. 2 shows the schematic cell structure. After a cleaning procedure including a KOH-based damage etch, a dielectric protection coating on the rear allows for a single-side texturing and phosphorus diffusion using POCl_3 as precursor gas resulting in a sheet resistance of 50–70 Ω/□. The phosphosilicate glass and the protection coating at the rear are removed simultaneously by an HF etch. Afterward, the dielectric passivation takes place. For group 1, the rear side of the wafers is coated with a 10-nm plasma-assisted ALD- Al_2O_3 layer using process parameters as described in [8], whereas for wafers of group 2 following a wet chemical cleaning, a dry thermal oxidation for 15 min at 900 °C is carried out, resulting in a 10–25-nm-thick SiO_2 layer on both surfaces. The rear side of the silicon wafers in group 3 is passivated by a plasma-enhanced chemical vapor

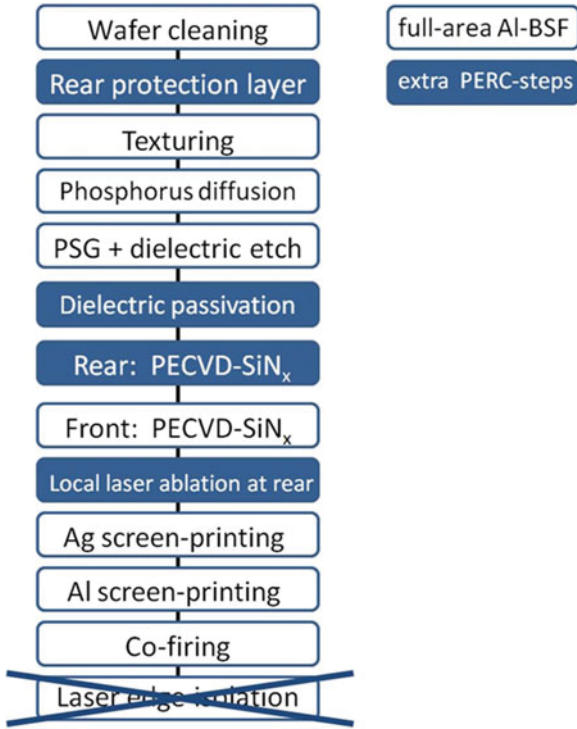


Fig. 1. Schematic of the process flows. The blue boxes show the additional steps for the PERC cells compared with the reference process for cells with a full-area Al-BSF. We vary the dielectric rear passivation between i) Al_2O_3 , ii) SiO_2 , and iii) silicon-rich SiN_y . Laser edge isolation is not required for the PERC cells, in contrast with the Al-BSF cells.

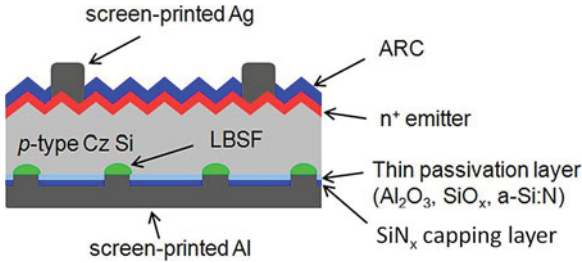


Fig. 2. Schematic of the PERC solar cells with screen-printed Ag front and Al rear contacts with i) $\text{Al}_2\text{O}_3/\text{SiN}_x$, ii) $\text{SiO}_2/\text{SiN}_x$, or iii) a-Si:N/ SiN_x rear passivation stacks. Note that cells ii) feature a thin thermally grown oxide below the SiN_x at the illuminated front side.

deposition (PECVD) silicon-rich silicon nitride layer SiN_y . Afterward, we deposit on top of the respective passivation layer at the rear a 200-nm-thick SiN_x layer (refractive index $n_{\text{SiN}} = 2.05$) by an inline microwave PECVD system (SiNA, Roth & Rau, Hohenstein-Ernstthal, Germany). The front side is also coated with an SiN_x layer of refractive index $n_{\text{SiN}} = 2.05$. The rear passivation stacks receive local line openings by a 532-nm laser with pulselengths of 10 ps. The line opening width is varied between 50 and 150 μm with pitches p ranging from 450 to 4000 μm . The screen-printed contacts to the emitter and to the base are formed by silver (Ag) and Al pastes, respectively. Due to variation between single and print-on-print screen printing, the Ag finger width varies between 70 and 140 μm . The aluminum rear contact is formed by standard full-area Al

screen printing. A drying process in a belt furnace (DO-HTO-5.200-210, Centrotherm, Blaubeuren, Germany) at about 200 °C completes each print process. A local BSF is formed during the co-firing step in an additional belt furnace (DO-FF-8.600-300, Centrotherm) with a set peak temperature of around 875 °C and belt velocities ranging from 5 to 6 m/min. Thereby, the contact formation by the Al paste occurs only in the openings of the passivating dielectric layer. Therefore, we vary the rear-side metallization fraction between 3% and 32%. Using a suitable Al paste, one achieves surface recombination velocities below the Al contacts of 600 cm/s on 2–3- Ω -cm p-type boron-doped Cz silicon [9]. According to the process flow in Fig. 1 displayed in white boxes, the full-area Al-BSF cells are manufactured for reference purposes. It is similar to the aforementioned introduced process flow for PERC cells, without the need to protect the rear from phosphorus diffusion and without deposition of structured passivation stacks at the rear. However, to avoid shunts, we apply laser edge isolation that is not required for PERC cells due to the single-side phosphorus diffusion.

III. COMPONENTS OF THE SERIES RESISTANCE

In this paper, we investigate the main cause of the high series resistance and focus on the impact of the rear-side contact geometry on the series resistance of the PERC solar cells. The front-side series resistance

$$R_{fs} = R_e + R_{c,e} + R_{fi} + R_{bus} \quad (2)$$

of the PERC cell consists of lumped contributions from the emitter sheet resistance R_e , the contacts to the emitter $R_{c,e}$, the front-side fingers R_{fi} , and the busbar R_{bus} , respectively. The total series resistance

$$R_s = R_{fs} + R_{edge} + R_b(f_{rear}) + R_{c,rear}(f_{rear}) \quad (3)$$

includes additional series resistance contributions from the wafer edges R_{edge} , the base resistance R_b , and from the contacts to the base $R_{c,rear}$. While R_{fs} depends only on the front side, the contact geometry and, hence, the metallization fraction f_{rear} at the rear has an impact on R_b and $R_{c,rear}$. The influence of the rear contact geometry on R_{edge} is in a first approximation neglected. A larger pitch increases R_b because majority carriers at the rear have to travel a longer lateral distance before reaching the rear contacts. In this contribution, we model R_b with the model of Gelmont and Shur for line-shaped contact patterns [10]–[12]:

$$R_b = \frac{p\rho}{2\pi} \ln \left(\frac{2 \left(\sqrt{\cosh(\pi a/4W)} + 1 \right)}{\sqrt{\cosh(\pi a/4W)} - 1} \right) + \rho W \left(1 - \exp \left(-\frac{W}{p} \right) \right) \quad (4)$$

which applies

$$\tanh \frac{\pi a}{4W} \leq \frac{1}{\sqrt{2}} \quad (5)$$

with the specific resistivity ρ and the thickness W of the silicon wafer. The line contact patterns are described by the width a and

TABLE I
SOLAR CELL PARAMETERS MEASURED UNDER STANDARD TESTING
CONDITIONS (125 mm × 125 mm PSEUDOSQUARE, ~180- μ m-THICK,
2–3 Ω -cm p-TYPE BORON-DOPED CZ SILICON)

| Cell | Rear side | f_{rear} | V_{oc} | J_{sc} | FF | pFF | η | R_s° |
|------|--|-------------------|-----------------|--------------------|------|-------|--------|----------------------------|
| | | % | mV | mA/cm ² | % | [%] | % | m Ω cm ² |
| A* | Al ₂ O ₃ /SiN _x | 12 | 652 | 38.9 | 75.1 | - | 19.0 | 1.3 |
| B* | SiO ₂ /SiN _x | 6 | 664 | 38.5 | 75.8 | - | 19.4 | 1.6 |
| C* | Al-BSF | 100 | 632 | 37.1 | 79.8 | - | 18.7 | 0.6 |
| 1 | Al ₂ O ₃ /SiN _x | 3.5 | 653 | 38.6 | 71.0 | 83.2 | 17.9 | 2.5 |
| 2 | Al ₂ O ₃ /SiN _x | 5 | 650 | 38.5 | 75.0 | 83.0 | 18.8 | 1.6 |
| 3 | Al ₂ O ₃ /SiN _x | 10 | 648 | 38.2 | 76.9 | 82.5 | 19.0 | 1.2 |
| 4 | Al ₂ O ₃ /SiN _x | 16.4 | 641 | 38.1 | 77.8 | 83.1 | 19.0 | 1.1 |

For cells A-C we apply PoP Ag print, for cell 1-4 single Ag print at the front.

* Independently confirmed at Fraunhofer ISE CalLab.

^o measured at ISFH applying FF -method.

the pitch p . The investigated rear contact patterns in this paper fulfill (5).

IV. RESULTS AND DISCUSSION

Table I shows the measured open-circuit voltage V_{oc} , short-circuit current density J_{sc} , fill factor FF , pseudo fill factor pFF , and conversion efficiency η of the respective best PERC solar cells with ALD Al₂O₃/PECVD SiN_x (cell A) and with thermally grown SiO₂/PECVD SiN_x (cell B) rear passivation stacks, in comparison with the data of the full-area Al-BSF reference (cell C). The one-sun performance of the processed cells is measured after deactivation of boron–oxygen-related recombination centers by simultaneously annealing and illuminating the cells with white light [13], [14]. This is applied to cell A–C fineline screen-printed Ag fingers at the front side. PERC solar cells with the passivation schemes fabricated according to the process flows shown in Fig. 1 achieve independently confirmed energy conversion efficiencies of 19.4% (SiO₂/SiN_x) and 19.0% (Al₂O₃/SiN_x), compared with 18.7% for the best full-area Al-BSF reference solar cell. Moreover, in Table I, the measured parameters of PERC solar cells with an Al₂O₃/SiN_x rear passivation stack and single screen-printed Ag fingers are shown (No. 1–4). Thereby, the metallization fraction at the rear f_{rear} ranges from 3.5% to 16.4%. Comparison of the single-printed cell 3 with PoP cell A with a similar f_{rear} reveals the limitation by the shadowing of the 130- μ m-wide Ag fingers. It corresponds to a decrease in J_{sc} of 0.6–0.8 mA/cm². In the first approximation, the wider finger width does not influence the series resistance. However, the fill factors FF of 75.1% (cell A) and 75.8% (B) are relatively moderate for the PERC cells when compared with the $FF = 79.8\%$ for the reference cell with a full-area AlBSF. The shunt resistances of all PERC solar cells are above 5 k Ω ·cm² and, therefore, high enough to be neglected.

A. R_s -Determination by Fill Factor Method

The smaller FF of the PERC solar cells is mainly caused by a larger series resistance of $R_s = 1.6 \Omega$ ·cm² (cell A), compared

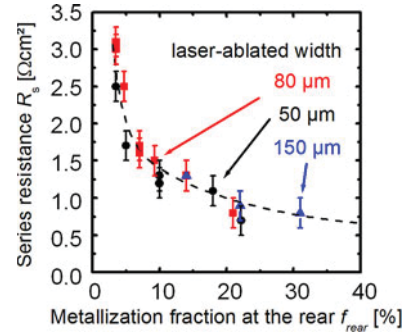


Fig. 3. Measured series resistance of the PERC solar cells with laser opening widths ranging from 50 to 150 μ m. The line is a guide to the eye.

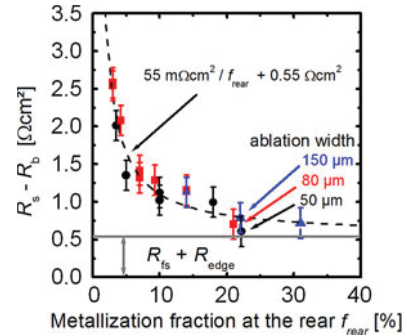


Fig. 4. $R_s - R_b$ of the PERC solar cells with different opening widths at the rear depending on f_{rear} . The corresponding fit provides R_{fs} and $R_{\text{c, rear}}$.

with $R_s = 0.6 \Omega$ ·cm² for the reference cell C as measured by the fill factor method [15], which describes the series resistance as

$$R_s = \frac{V_{\text{oc}}}{J_{\text{sc}}} \cdot \left(1 - \frac{FF}{pFF} \right). \quad (6)$$

V_{oc} , J_{sc} , and FF are determined from the I - V characteristic of the illuminated solar cell and the pseudo fill factor pFF from the J_{sc} - V_{oc} characteristic.

Fig. 3 shows the measured series resistances R_s as determined from (6) of the PERC solar cells with laser-ablated opening widths in the rear-side passivation stacks of 50, 80, and 150 μ m as a function of the rear metallization fraction f_{rear} . The conversion efficiencies range from 16% to 19.4%. Investigations on the width of line-shaped contact openings show an enlargement of 20–30 μ m at each contact side after the firing process, which is included in f_{rear} . We observe a strong dependence of the measured series resistance R_s on the metallization fraction at the rear. With increasing f_{rear} from 3% to 32%, R_s decreases from 3.1 to 0.8 Ω ·cm².

In order to separate the various contributions to the series resistance, Fig. 4 shows the difference between the measured series resistance R_s and the calculated series resistance contribution of the base R_b [see (4)] by applying (3). We thus fit this difference by

$$R_s - R_b(f_{\text{rear}}) = \frac{55 \text{ m}\Omega \cdot \text{cm}^2}{f_{\text{rear}}} + 0.55 \Omega \cdot \text{cm}^2 \quad (7)$$

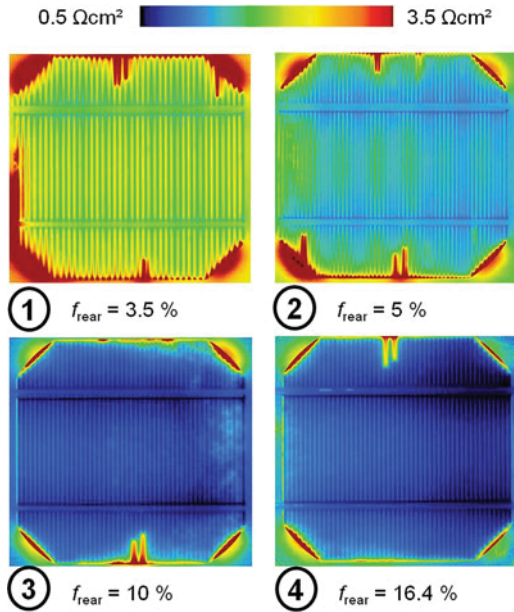


Fig. 5. PL- R_s measurements of PERC solar cells with $\text{Al}_2\text{O}_3/\text{SiN}_x$ rear passivation stack. The numeration corresponds to cell numbers of Table II. The 50- μm -wide laser line openings are separated by four different pitches, resulting in rear metallization fractions from 3.5% to 16.4%.

where in the first approximation, all the experimental data points are well described.

Applying (2), we thus find for the f_{rear} -independent contributions of the front side and the edges

$$R_e + R_{c,e} + R_{\text{fi}} + R_{\text{bus}} + R_{\text{edge}} = 0.55 \Omega \cdot \text{cm}^2 \quad (8)$$

and using (1) results in an effective specific contact resistivity for the local Al contacts of

$$\rho_c = (55 \pm 10) \text{ m}\Omega \cdot \text{cm}^2. \quad (9)$$

The results indicate that in the first-order approximation, the effective specific contact resistivity of local screen-printed Al contacts does not depend on the contact size. However, in Fig. 4, it seems that ρ_c increases slightly with the contact width that corresponds to observations of Urrejola *et al.* [7]. However, some of this seems to be only a small-scale effect. Further experiments have to be conducted to verify this result with larger statistics.

B. R_s -Determination by PL Measurements

In the following, we focus on another method to determine the series resistance. Fig. 5 shows mappings of the local series resistance based on PL measurements [16] for the PERC solar cells 1–4 in Table I. Confirming the strong impact of the rear metallization on R_s , the area-averaged series resistance decreases from 2.3 ($f_{\text{rear}} = 3.5\%$) to 0.9 $\Omega \cdot \text{cm}^2$ ($f_{\text{rear}} = 16.4\%$).

Fig. 6 shows the area-averaged series resistances from PL measurements at three defined areas at each solar cell, as shown in the inset.

- 1) whole cell area (black symbols in Fig. 6);
- 2) wafer center (red symbols in Fig. 6);
- 3) near the busbar (blue symbols in Fig. 6).

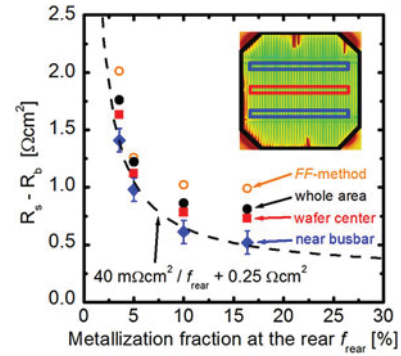


Fig. 6. Area-averaged R_s measured by PL at different locations of the PERC solar cells reduced by the contribution of the base R_b depend strongly on f_{rear} . Measurement results of the entire cell area are shown in black, of the cell center in red, and nearby the busbars in blue symbols. For comparison, measurement results from the FF method are shown with opened orange symbols.

Thereby, we subtract the contribution of the base R_b regarding (4) for each measurement for the various f_{rear} . We observe a slightly smaller full-area averaged R_s data (black) in comparison with measured R_s from the FF method (orange). Comparing the full-area averaging results (black) with the data in the center of the solar cells (red), we notice in a first order a systematic deviation of about 0.1 $\Omega \cdot \text{cm}^2$. That increase is mainly caused by the strong increase of the local series resistance at the wafer edges. Therefore, R_{edge} of approximately 0.1 $\Omega \cdot \text{cm}^2$ is influenced, e.g., by the screen design and requires further optimization. Comparing R_s from the wafer center (red) with the R_s in the busbar area (blue) reveals a constant difference. That is attributed to the front-side fingers R_{fi} of about 0.2 $\Omega \cdot \text{cm}^2$. Contributions of R_{edge} and R_{fi} are minimized when we measure the area-averaged R_s nearby the busbars and somewhat away from the wafer edges (blue symbols in Fig. 6). These experimental data points are according to (7)–(9) well described by a potential fit resulting in a sum of the residual f_{rear} -independent contributions from the emitter, the front contact, and the busbar of 0.25 $\Omega \cdot \text{cm}^2$, and by using (1), we find

$$\rho_c = (40 \pm 10) \text{ m}\Omega \cdot \text{cm}^2. \quad (10)$$

This value agrees well with the contact resistivity of $(55 \pm 10) \text{ m}\Omega \cdot \text{cm}^2$ obtained from the FF method. Accordingly, the contribution to series resistance associated with the screen-printed contact resistance is, therefore, given by

$$R_{c,\text{rear}} = \frac{40 \text{ m}\Omega \cdot \text{cm}^2}{f_{\text{rear}}}. \quad (11)$$

The sum of the f_{rear} -independent contributions to the series resistance deduced from PL measurements of 0.55 $\Omega \cdot \text{cm}^2$ fits also well with the equivalent determined by the FF method from (8).

Table II shows for the PERC solar cell 2 from Table I with 18.8% energy conversion efficiency the split-up of the series resistance R_s deduced from PL measurements. R_s is increased to 1.6 $\Omega \cdot \text{cm}^2$ compared with the reference cell with a full-area Al-BSF and $R_s = 0.6 \Omega \cdot \text{cm}^2$ (cell C in Table I). The high R_s of the PERC cell is attributed to the high contribution of the base

TABLE II
FROM PL MEASUREMENTS DEDUCED SERIES RESISTANCE CONTRIBUTIONS OF
THE PERC SOLAR CELL 2 IN TABLE I ($f_{\text{rear}} = 5\%$)

| R_s contributions | Symbols | PERC [Ωcm^2] |
|--------------------------------|----------------------------------|---------------------------------|
| Emitter, front contact, busbar | $R_e + R_{c,e} + R_{\text{bus}}$ | 0.25 |
| Wafer edges | R_{edge} | 0.1 |
| Screen-printed Ag finger | R_{fi} | 0.2 |
| Base | R_b | 0.3 |
| Rear contact | $R_{c,\text{rear}}$ | 0.8 |
| Sum | | 1.65 |

The measured R_s of $1.6 \Omega\text{-cm}^2$ fits well with the sum of the single contributions.

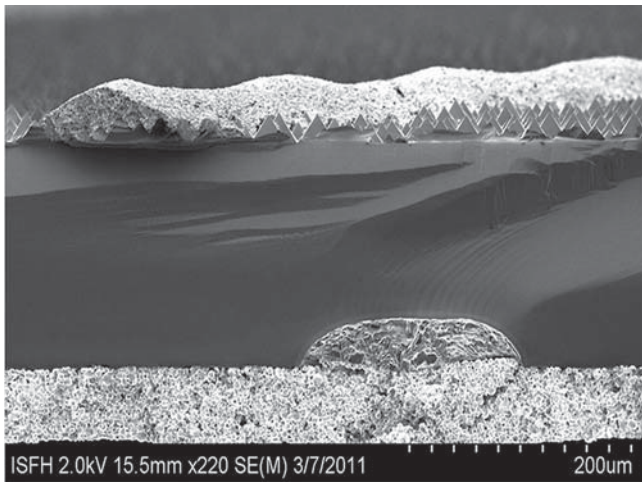


Fig. 7. SEM image of the cross section of a PERC solar cell with pyramid texture at the top with a screen-printed Ag finger. The local rear contact opening features an up to $40\text{-}\mu\text{m}$ -deep Al-Si eutectic layer above a homogeneous Al-BSF which is grown epitaxial during the cool down after the firing step. The cross fraction is not perpendicular to the line directions.

R_b of approximately $0.3 \Omega\text{-cm}^2$. The main contribution to R_s , however, is the high contact resistance at the cell rear of $R_{c,\text{rear}} = 0.8 \Omega\text{-cm}^2$. For full-area Al-BSF solar cells, the contributions R_b and $R_{c,\text{rear}}$ are small, e.g., $< 0.1 \Omega\text{-cm}^2$. Accordingly, $R_{c,\text{rear}}$ reduction is essential for further efficiency improvements.

V. CONCLUSION

To reduce the series resistance, the contribution of the rear contact $R_{c,\text{rear}}$ has to be minimized. Therefore, according to (1), one can increase the rear metallization fraction f_{rear} . However, it would result in an increased rear surface recombination velocity and a decreased reflectance and, therefore, limits V_{oc} and J_{sc} , as shown for cells 1–4 in Table I. The other possibility to decrease $R_{c,\text{rear}}$ is to decrease the specific contact resistivity ρ_c . In comparison with Al paste fired on bare Si with $\rho_c = 10 \text{ m}\Omega\text{-cm}^2$ [6], the obtained values for local screen-printed PERC contacts of $\rho_c = 40\text{--}55 \text{ m}\Omega\text{-cm}^2$ are relatively high and need to be reduced. Assuming $\rho_c = 10 \text{ m}\Omega\text{-cm}^2$ for the local rear contact for solar cell B in Table I, it would result in an FF increase from 75.8% to 78% and, therefore, in an efficiency increase to 20%.

Fig. 7 shows a cross section scanning electron microscopy (SEM) image of a PERC solar cell. Every investigated local

rear contact features an enlargement of $20\text{--}30 \mu\text{m}$ at each contact side. The line cavities are up to $40 \mu\text{m}$ deep. By locally ablation of the dielectric layers with picoseconds laser [17] and using a suitable screen-printed Al paste, these cavities are fullfilled homogenously with an Al-Si eutectic layer whereby an about $7\text{-}\mu\text{m}$ -thick Al-BSF is formed underneath [9]. Therefore, the microstructure of the local contacts differs substantially from the conventional full-area Al-BSF contact. The increase in the effective specific contact resistivity from 10 to $40\text{--}55 \text{ m}\Omega\text{-cm}^2$ could result from the significantly deeper Al-Si eutectic layer compared with $1\text{--}10 \mu\text{m}$ for the conventional full-area Al-BSF solar cells. However, further experiments have to be conducted to identify the physical background of the significant higher specific contact resistivity of screen-printed local rear contacts.

VI. SUMMARY

In this paper, we analyze the fill factor loss in large-area screen-printed solar cells with passivated homogenous emitter and rear on p-type $2\text{--}3\text{-}\Omega\text{-cm}$ boron-doped Cz-silicon wafers achieving energy conversion efficiencies of up to 19.4%. By variation of the rear contact geometry, we separate the different contributions to the series resistance. Our analysis shows that a major impact on the increased series resistance is the contribution of the rear contact. It reveals that the effective specific contact resistivity of local screen-printed PERC contacts is relatively high with $40\text{--}55 \text{ m}\Omega\text{-cm}^2$ and has, therefore, the potential for improvement in order to achieve cell efficiencies above 20%.

ACKNOWLEDGMENT

The authors would like to thank A. Lohse for processing the solar cells and T. Neubert for providing his assistance with sample preparation. They gratefully acknowledge fruitful discussions with J. Schmidt.

REFERENCES

- [1] S. Narasimha and A. Rohatgi, "Optimized aluminum back surface field techniques for silicon solar cells," in *Conf. Rec. 26th IEEE Photovoltaic Spec. Conf.*, Anaheim, CA, 1997, pp. 63–66.
- [2] S. Peters, "Rapid thermal processing of crystalline silicon materials and solar cells," Ph.D. dissertation, Univ. Constance, Konstanz, Germany, 2004, pp. 62–72.
- [3] A. W. Blakers, A. Wang, A. M. Milne, J. Zhao, and M. A. Green, "22.8% efficient silicon solar cell," *Appl. Phys. Lett.*, vol. 55, pp. 1363–1365, 1989.
- [4] S. Gatz, H. Hannebauer, R. Hesse, F. Werner, A. Schmidt, T. Dullweber, J. Schmidt, K. Bothe, and R. Brendel, "19.4%-efficient large-area fully screen-printed silicon solar cells," *Phys. Status Solidi RRL*, vol. 5, no. 4, pp. 147–149, 2011.
- [5] M. Melczarsky, G. Gallego Garcia, N. Posthuma, E. Van Kerschaver, and G. Beaucarne, "Contact resistance measurement techniques for Ag thick-film screen-printed contacts to solar cells," in *Proc. 34th IEEE Photovoltaic Spec. Conf.*, Philadelphia, PA, 2009, pp. 960–963.
- [6] A. Rohatgi, S. Narasimha, and D. S. Ruby, "Effective passivation of the low resistivity silicon surface by a rapid thermal oxide/PECVD silicon nitride stack and its application to passivated rear and bifacial Si solar cells," in *Proc. 2nd World Conf. Photovoltaic Energy Convers.*, Vienna, Austria, 1998, pp. 1566–1569.
- [7] E. Urrejola, K. Peter, H. Plagwitz, and G. Schubert, "Al-Si alloy formation in narrow p-type Si contact areas for rear passivated solar cells," *J. Appl. Phys.*, vol. 107, no. 12, pp. 124516-1–124516-7, 2010.

- [8] J. Schmidt, B. Veith, and R. Brendel, "Effective surface passivation of crystalline silicon using ultrathin Al_2O_3 films and $\text{Al}_2\text{O}_3/\text{SiN}_x$ stacks," *Phys. Status Solidi RRL*, vol. 3, no. 9, pp. 287–289, 2009.
- [9] S. Gatz, K. Bothe, J. Mueller, T. Dullweber, and R. Brendel, "Analysis of local Al-doped back surface fields for high efficiency screen-printed solar cells," *Energy Procedia*, vol. 8, pp. 318–323, 2011.
- [10] B. Gelmont and M. Shur, "Spreading resistance of a round ohmic contact," *Solid-State Electron.*, vol. 36, no. 2, pp. 143–146, 1993.
- [11] B. Gelmont, M. S. Shur, and R. J. Mattauch, "Disk and stripe capacitance," *Solid-State Electron.*, vol. 38, no. 3, pp. 731–734, 1995.
- [12] H. Plagwitz, "Surface passivation of crystalline silicon solar cells by amorphous silicon films," Ph.D. dissertation, Univ. Hannover, Hannover, Germany, 2007.
- [13] A. Herguth, G. Schubert, M. Kaes, and G. Hahn, "Avoiding boron–oxygen related degradation in highly boron-doped Cz silicon," in *Proc. 21st Eur. Photovoltaic Solar Energy Conf.*, Dresden, Germany, 2006, pp. 530–537.
- [14] B. Lim, K. Bothe, and J. Schmidt, "Deactivation of the boron–oxygen recombination center in silicon by illumination at elevated temperature," *Phys. Status Solidi RRL*, vol. 2, no. 3, pp. 93–95, 2008.
- [15] M. A. Green, *Solar cells: Operating Principles, Technology and System Applications*. Sydney, Australia: Univ. New South Wales, 1998, p. 96.
- [16] T. Trupke, E. Pink, R. A. Bardos, and M. D. Abbott, "Spatially resolved series resistance of silicon solar cells obtained from luminescence imaging," *Appl. Phys. Lett.*, vol. 90, pp. 093506-1–093506-3, 2007.
- [17] J. Müller, K. Bothe, S. Gatz, H. Plagwitz, G. Schubert, and R. Brendel, "Recombination at local aluminum-alloyed silicon solar cell base contacts by dynamic infrared lifetime mapping," *Energy Procedia*, vol. 8, pp. 337–342, 2011.



Sebastian Gatz studied in Regensburg, Germany; Dublin, Ireland; and Munich, Germany. In 2006, he received the Diploma degree in physics from the Technical University München, Munich, Germany. He has been working toward the Ph.D. degree with the Institute for Solar Energy Research Hamelin, Emmerthal, Germany, since 2007.

He was with the Department of Physics, Trinity College Dublin, where he was focused on the physics of fluids, during 2002–2003. During 2005–2006, he was with the Experimental Semiconductor Physics

Group of Prof. M. Stutzmann with the Walter-Schottky-Institute, Garching, Germany, where he investigated the aluminum-induced crystallization and low-temperature epitaxy of Silicon-Germanium for photovoltaic applications. In the Production processes group of Dr. T. Dullweber, he does research on front- and rear-side passivated screen-printed solar cells.



Thorsten Dullweber received the Ph.D. degree in electrical engineering from the University of Stuttgart, Stuttgart, Germany, in 2002.

From 2001 to 2009, he was a Project Leader with Siemens, Infineon, and Qimonda, mainly in technology development and the transfer of dynamic random access memory chips. In 2009, he joined the Institute for Solar Energy Research Hamelin, Emmerthal, Germany, where he is currently leading the R&D group "solar cell production processes," which focuses on process and efficiency improvements of industrial-type screen-printed silicon solar cells.



Rolf Brendel studied in Freiburg and Heidelberg, Germany, and with the University of Sussex, Brighton, U.K. He received the Diploma degree in physics in nuclear fusion research in 1987 and the 1st German State Board Examination in Mathematics (teacher degree level) in 1988. In 1992, he received the Ph.D. degree from the University of Erlangen, Erlangen, Germany, for his research on infrared spectroscopy.

He then joined the Max Planck Institute for Solid State Research, Stuttgart, Germany, to study the physics of thin-film silicon solar cells and the thermodynamics of photovoltaic power conversion. In 1997, he became the Head of the Division for Thermosensors and Photovoltaics with the Bavarian Center for Applied Energy Research, where he was involved in research on imaging diagnostics of solar cells. In 2004, he joined the Institute of Solid State Physics, Leibniz University of Hanover, Hanover, Germany, as a Professor. He is also the Director of the Institute for Solar Energy Research in Hamelin, Emmerthal, Germany.